Solar forcing of Florida Straits surface salinity during the early Holocene

Matthew W. Schmidt,[1] William A. Weinlein,[1] Franco Marcantonio,[2] and Jean Lynch-Stieglitz[3]

Received 12 January 2012; revised 17 April 2012; accepted 4 June 2012; published 19 July 2012.

[1] Previous studies showed that sea surface salinity (SSS) in the Florida Straits as well as Florida Current transport covaried with changes in North Atlantic climate over the past two millennia. However, little is known about earlier Holocene hydrographic variability in the Florida Straits. Here, we combine Mg/Ca-paleothermometry and stable oxygen isotope measurements on the planktonic foraminifera *Globigerinoides ruber* (white variety) from Florida Straits sediment core KNR166–2 JPC 51 (24° 24.70′ N, 83° 13.14′ W, 198 m deep) to reconstruct a high-resolution (~25 yr/sample) early to mid Holocene record of sea surface temperature and $\delta^{18}O_{SW}$ (a proxy for SSS) variability. After removing the influence of global $\delta^{18}O_{SW}$ change due to continental ice volume variability, we find that early Holocene SSS enrichments are associated with increased evaporation/precipitation ratios in the Florida Straits during periods of reduced solar forcing, increased ice rafted debris in the North Atlantic and the development of more permanent El Niño–like conditions in the eastern equatorial Pacific. When considered with previous high-resolution reconstructions of Holocene tropical atmospheric circulation changes, our results provide evidence that variations in solar forcing over the early Holocene had a significant impact on the global tropical hydrologic cycle.

Citation: Schmidt, M. W., W. A. Weinlein, F. Marcantonio, and J. Lynch-Stieglitz (2012), Solar forcing of Florida Straits surface salinity during the early Holocene, *Paleoceanography*, *27*, PA3204, doi:10.1029/2012PA002284.

1. Introduction

[2] There is a critical need to understand the mechanisms involved in climate dynamics over the current interglacial period in order to better predict how climate may evolve over the next few centuries. Prior studies have shown that the North Atlantic has experienced a number of quasiperiodic climate cycles over the last few millennia, the most recent being the Little Ice Age (LIA) from ~150 to 450 yrs BP and the Medieval Warm Period (MWP) from ~700 to 1500 yr BP [*deMenocal et al.*, 2000; *Lund et al.*, 2006; *Richey et al.*, 2009]. However, very little is known about submillennial-scale climate oscillations during earlier parts of the Holocene. In addition, the driver of these Holocene climate oscillations is still unknown. While some researchers argue that external forcing (solar variability) is responsible for Holocene climate cycles [*Marchitto et al.*, 2010], others argue for an internal mechanism [*Cane and Clement*, 1999; *Clement and Cane*, 1999].

[3] The Florida Current makes up a major component of the northward flowing Gulf Stream system, and thus forms an important link between the tropics and the high-latitude North Atlantic. *Lund and Curry* [2006] showed that climate variability in the Florida Straits is linked to high-latitude climate change and *Lund et al.* [2006] found that Florida Current transport may be coupled to changes in North Atlantic Meridional Overturning Circulation (AMOC) variability over the past two millennia. In particular, the period of reduced AMOC and cooler climate in the North Atlantic during the LIA was associated with drier conditions in the Florida Straits as the Hadley circulation cells and the Intertropical Convergence Zone (ITCZ) shifted southward of its modern position.

[4] To determine if the Florida Straits experienced millennial- and centennial-scale climate oscillations similar to the LIA during the early Holocene, we generated a high-resolution record of early Holocene sea surface temperature (SST) and sea surface salinity (SSS) variability using a sediment core recovered from the Florida Margin of the Florida Straits, KNR166–2 JPC 51 (24° 24.70′ N, 83° 13.14′ W, 198 m deep) (Figure 1). By combining Mg/Ca-paleothermometry and stable oxygen isotope measurements on the planktonic foraminifera *Globigerinoides ruber* (white variety), we reconstruct a high-resolution (~25 yr/sample) early to mid Holocene record (9.1 to 6.2 kyr) and a lower resolution

[1]Department of Oceanography, Texas A&M University, College Station, Texas, USA.
[2]Department of Geology and Geophysics, Texas A&M University, College Station, Texas, USA.
[3]School of Earth and Atmospheric Sciences, Georgia Institute of Technology, Atlanta, Georgia, USA.

Corresponding author: M. W. Schmidt, Department of Oceanography, Texas A&M University, College Station, TX 77843, USA. (schmidt@ocean.tamu.edu)

0883-8305/12/2012PA002284

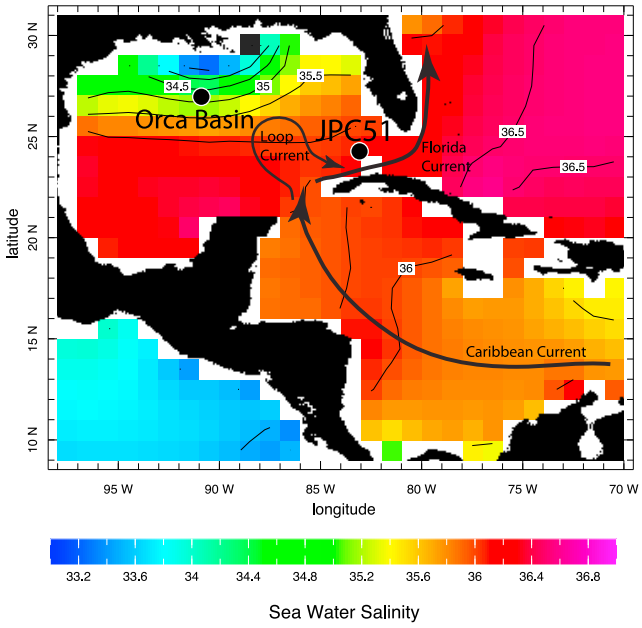

Figure 1. The location of KNR166–2 JPC 51 (24° 24.70′ N, 83° 13.14′ W, 198 m deep) on the western margin of the Florida Straits and modern annual sea surface salinity in western tropical Atlantic and the Gulf of Mexico [*Antonov et al.*, 2010]. As discussed in the text, core KNR166–2 79 GGC is located at nearly the same location as JPC 51. Also noted is the location of the Orca Basin, where core MD02–2550 was recovered in the northern Gulf of Mexico. Black arrows indicate the major ocean currents in the region.

(∼150 yr/sample) mid to late Holocene record (6.2 to 1.4 kyr) of $\delta^{18}O_{SW}$ variability in the Florida Straits. After correcting the $\delta^{18}O_{SW}$ record for global changes in $\delta^{18}O_{SW}$ due to continental ice volume variability, the ice volume free $\delta^{18}O_{SW}$ record can be used as a proxy for past changes in SSS.

2. Oceanographic Setting

[5] Waters from the Caribbean are directly connected with the Florida Straits via flow through the Yucatan Channel [*Maul and Vukovich*, 1993; *Murphy et al.*, 1999]. As such, waters in the Florida Straits are predominantly characteristic of the Caribbean [*Brunner*, 1982; *Lynch-Stieglitz et al.*, 1999] and form an important link between waters of the Caribbean, Gulf of Mexico and North Atlantic (Figure 1).

[6] The modern seasonal SST cycle in the Florida Straits varies from 25.0 to 26.0°C from December through March to 29.0 to 29.4°C from July to mid-September, with a modern average annual SST of 27.5°C [*Locarnini et al.*, 2006]. Mesoscale cyclonic eddies form near the Dry Tortugas during periods of strong Loop Current development [*Fratantoni et al.*, 1998]. These frontal eddies associated with the Loop Current can persist for about 100 days and their presence acts to cool SST in the Florida Straits during winter and spring when surface temperatures in the Gulf of Mexico are cooler than in the Florida Current [*Fratantoni et al.*, 1998].

[7] In the modern tropical Atlantic and Caribbean region, seasonal rainfall variability is primarily controlled by the annual migration of the ITCZ between 15°N and 5°S [*Waliser and Gautier*, 1993]. Therefore, evaporation/precipitation (E/P) ratios decrease during the boreal summer months when the ITCZ is located farthest to the north and increase during the cool, dry season as the ITCZ migrates southward during boreal winter [*Stidd*, 1967]. Modern annual SSS in the Florida Straits varies from 36.1 to 36.2 from January to June to ∼35.9 from August to December, with a modern average annual SSS of ∼36.1 [*Antonov et al.*, 2006].

3. Materials and Methods

3.1. Age Model Development

[8] To develop an age model for JPC 51 across the Holocene, seven intervals were sampled for radiocarbon analysis (Table 1 and Figure S1 in the auxiliary material).[1] Five of the intervals chosen for radiocarbon analysis span the high-resolution section of our early Holocene record. Radiocarbon analyses were conducted using 3.4 to 5.5 mg of *G. ruber* and *Globigerinoides sacculifer* shells collected from the >355 μm size fraction. These samples were analyzed at the National Ocean Sciences Accelerator Mass Spectrometry Facility of the Woods Hole Oceanographic Institution in Massachusetts. Raw ^{14}C ages were converted to calendar age using CALIB 6.0 using the standard reservoir age of 400 years for surface waters (Table 1) (M. Stuiver et al., Calib calibration program, version 6.0, 2011). Linear interpolation between ^{14}C-dated control points yields Holocene sedimentation rates in JPC 51 ranging from 60 to 188 cm/kyr. The upper 295 cm of JPC 51 corresponds to the time interval between 6.21 to 1.48 kyr and the lower 254.25 cm corresponds to the time interval between 9.16 to 6.21 kyr. Based on our age model, the core has maximum sedimentation rates of 141 to 188 cm/kyr from 8.0 to 7.3 kyr. Sedimentation rates range from 60 to 83 cm/kyr in the section of the core corresponding to 7.3 to 1.4 kyr. The core was sampled every 2 cm from 554.5 to 300.5 cm (corresponding to our high-resolution time interval spanning the early Holocene from 9.16–6.21 kyr) and every 8 cm from 296.5 cm to the core top.

3.2. Stable Isotope Analysis

[9] Sediment from each core interval was dried overnight at ∼50°C, then weighed and disaggregated in ultra clean

[1] Auxiliary materials are available in the HTML. doi:10.1029/2012PA002284.

Table 1. AMS ^{14}C and Calendar Ages

Core	Depth (cm)	CAMS Number	^{14}C Age	Error (years)	Calendar Age (kyr B.P.)	Error (years)
JPC 51	5.25	40017	1940	40	1.49	110
JPC 51	159.25	49009	4040	45	4.07	146
JPC 51	312.25	40018	5970	60	6.40	131
JPC 51	394.5	76076	6880	40	7.39	87
JPC 51	480.25	40019	7520	70	7.99	152
JPC 51	494.5	76077	7610	35	8.07	90
JPC 51	632.25	40020	9690	75	10.56	194

water for 6 h on a shaker table. To collect the coarse fraction, samples were wet-sieved using a 63 μm mesh. For each interval, 80 individual *G. ruber* (white variety) specimens were collected from the 255 to 350 μm size fraction. The 255 to 350 μm size fraction limitation was used to minimize ontogenetic and growth rate effects on shell geochemistry [*Lea et al.*, 2000; *Spero et al.*, 2003]. To ensure an unbiased estimation of the average δ^{18}O value for a given interval, we used 17 to 25 *G. ruber* shells for each individual stable isotope analysis. Samples were sonicated in methanol for 6 s, then crushed and homogenized prior to analysis. A 100 to 150 μg split of the sample was then analyzed for stable isotopes in J. Lynch-Stieglitz's laboratory at the Georgia Institute of Technology on a Finnigan MAT253 stable isotope ratio mass spectrometer with a Kiel Device. Raw δ^{18}O values were standardized using NBS-19 and Venato 690 (an in-house standard).

3.3. Minor and Trace Metal Analysis

[10] For minor and trace metal analysis, 45 to 60 *G. ruber* shells ($\sim$580 μg) from each core interval were gently crushed between glass plates under a microscope, homogenized and then split. To maintain trace metal clean conditions, the samples were then cleaned according to the procedures of *Lea et al.* [2000] in a laminar flow clean bench. The cleaning process included sonication in both ultra clean water and methanol to remove clays, a hot water bath in reducing agents to remove metal oxides and a hot water bath in an oxidizing solution to remove organic matter. Finally, the samples were transferred to acid cleaned vials and leached in weak nitric acid. The samples were analyzed in duplicate at Texas A&M University on a Thermo Scientific Element XR High Resolution Inductively Coupled Plasma Mass Spectrometer (HR-ICP-MS) using isotope dilution, as outlined in *Lea and Martin* [1996]. A suite of elements including Na, Mg, Ca, Sr, Ba, U, Al, Fe and Mn, were analyzed and reported as metal/Ca ratios. All geochemical data is archived at the NOAA National Climate Data Center at: http://www.ncdc.noaa.gov/paleo/paleo.html.

3.4. Calculations

[11] Foraminiferal Mg/Ca:temperature relationships have been derived from a combination of experimental, core top, and sediment trap calibrations [*Anand et al.*, 2003; *Dekens et al.*, 2002; *Nürnberg et al.*, 1996]. Because it is unlikely that dissolution is an issue in the shallow core selected for this study, we utilized the non-depth corrected Mg/Ca:SST calibration of *Anand et al.* [2003] to estimate calcification temperatures in JPC 51:

$$\mathrm{Mg/Ca} = 0.38\exp(0.09{*}\mathrm{T})(\mathrm{error}\ \pm 0.5^{\circ}\mathrm{C}) \quad (1)$$

This equation was derived from the measurement of Mg/Ca ratios in planktonic foraminifera collected from sediment traps in the Sargasso Sea and modern SST data. The estimated 1σ error on this relationship is between $\pm$0.5 to 1.0°C [*Anand et al.*, 2003]. It is important to note that equation (1) is identical to the previously published Atlantic *G. ruber* Mg/Ca:SST relationship developed from core tops in *Dekens et al.* [2002], but without the depth correction term. Given the shallow depth of JPC 51 and the lack of dissolution in the core, we did not feel a depth correction term was needed. Although a recent study by *Arbuszewski et al.* [2010] suggests that SSS has a major impact on foraminiferal Mg/Ca ratios, we find no evidence of this influence on our reconstructed Mg/Ca-SST record from JPC 51 (see auxiliary material).

[12] The oxygen isotopic composition of foraminiferal calcite is a function of the temperature and the ambient isotopic composition of the seawater ($\delta^{18}O_{SW}$) in which it precipitates its shell. If the temperature component is accounted for, foraminiferal calcite can be used to estimate past changes in SSS because $\delta^{18}O_{SW}$ covaries linearly with SSS [*Fairbanks et al.*, 1992]. Based on this concept, numerous studies have developed and refined a multiproxy geochemical approach in which calibrated Mg/Ca ratios from planktonic foraminifera shells are used to estimate past SSS variability [*Carlson et al.*, 2008; *Lea et al.*, 2000; *Lund and Curry*, 2006; *Schmidt et al.*, 2004; *Weldeab et al.*, 2007].

[13] *Lea et al.* [2000] and *Schmidt et al.* [2004] found that the low-light temperature:δ^{18}O relationship determined for *Orbulina universa* in laboratory culture experiments [*Bemis et al.*, 1998] yields excellent results when applied to fossil *G. ruber* (white variety) to calculate modern $\delta^{18}O_{SW}$ in the equatorial Pacific and Caribbean. Using the *Bemis et al.* [1998] $\delta^{18}O_C$:SST relationship,

$$\mathrm{T}(^{\circ}\mathrm{C}) = 16.5 - 4.80\left(\delta^{18}O_C - \left(\delta^{18}O_{SW} - 0.27‰\right)\right)(\mathrm{error} \pm 0.7^{\circ}\mathrm{C}) \quad (2)$$

$\delta^{18}O_C$ values and Mg/Ca SST values were combined to calculate $\delta^{18}O_{SW}$.

3.5. Estimating SSS Change From $\delta^{18}O_{SW}$

[14] Changes in continental ice volume also affect global $\delta^{18}O_{SW}$ values. If this effect can be accounted for, the resulting ice volume free $\delta^{18}O_{SW}$ ($\delta^{18}O_{IVF\text{-}SW}$) record can be used to estimate regional salinity change. Sea level has risen by $\sim$25 m over the last 10 kyr due to the melting of polar ice sheets [*Bard et al.*, 1990; *Cutler et al.*, 2003; *Edwards et al.*, 1993]. Because continental ice is isotopically depleted in δ^{18}O, addition of this meltwater has changed the average global ocean $\delta^{18}O_{SW}$ value by $\sim$0.20 ‰ over the last 10 kyr. In order to correct for this continental ice volume effect, we used a compilation of sea level records for the last 10 kyr [*Bard et al.*, 1990; *Cutler et al.*, 2003; *Edwards et al.*, 1993]. Assuming a one meter increase in sea level change equates to a change of -0.008 ‰ in global $\delta^{18}O_{SW}$ [*Siddall et al.*, 2003], we subtracted global changes in $\delta^{18}O_{SW}$ from our calculated Florida Straits $\delta^{18}O_{SW}$ record, resulting in the regional $\delta^{18}O_{IVF\text{-}SW}$ record.

3.6. Error Analysis

[15] The analytical precision for the δ^{18}O analyses is less than $\pm$0.07 ‰. The long-term analytical reproducibility of a synthetic, matrix-matched Mg/Ca standard analyzed over the course of this study is $\pm$0.48%, and the pooled standard deviation of the replicate Mg/Ca analyses is $\pm$3.58% (1 SD, 186 degrees of freedom) based on 164 analyzed intervals. When combined with the error on calibration equation (1), the analytical error associated with the Mg/Ca measurements contributes an additional 0.4°C of uncertainty. To calculate the combined $\pm$1σ error on the smoothed SST record on Figures 2b and 3, we used the following equation:

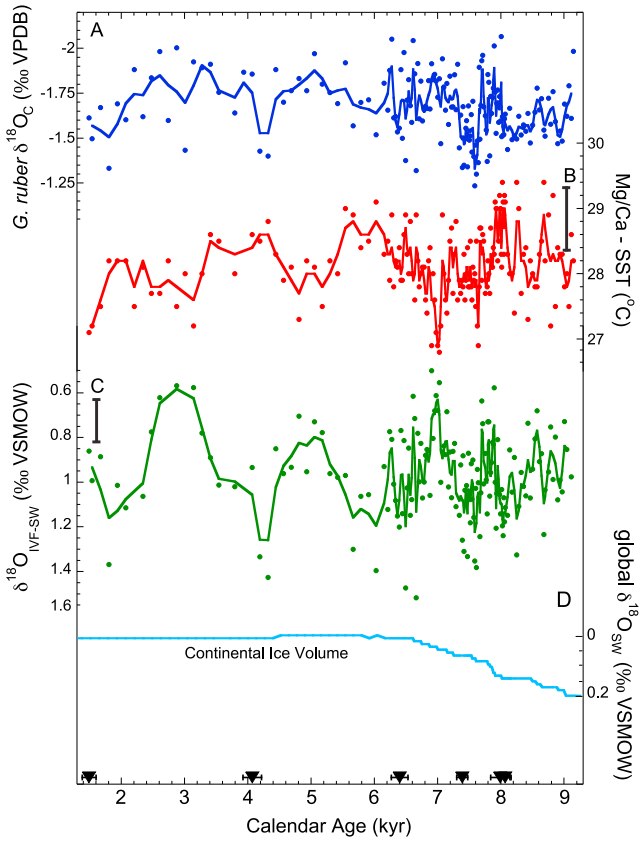

Figure 2. (a) *G. ruber* (white variety) $\delta^{18}O_C$ (blue line is a weighted 3-point smooth through the raw data points represented as blue circles) and (b) the *G. ruber* Mg/Ca-SST (red line is a weighted 3-point smooth through the raw data points represented as red circles) records from JPC 51. Measured Mg/Ca ratios (mmol/mol) were converted to SST using the planktonic relationship Mg/Ca = 0.38 exp 0.09 (SST) [*Anand et al.*, 2003]. The combined calibration and analytical error ($\pm 1\sigma$) on the smoothed record is shown as the black bar near the *y* axis. (c) Calculated ice volume free $\delta^{18}O_{SW}$ ($\delta^{18}O_{IVF\text{-}SW}$) record (green line is a weighted 3-point smooth through the raw data points represented as green circles) generated using the Mg/Ca-SST, the following $\delta^{18}O_C$: SST relationship: $T(°C) = 16.5 - 4.80(\delta^{18}O_C - (\delta^{18}O_{SW} - 0.27‰))$ [*Bemis et al.*, 1998], and by subtracting (d) the global $\delta^{18}O_{SW}$ change due to continental ice volume variability based on a compilation of sea level records for the last 10 kyr [*Bard et al.*, 1990; *Cutler et al.*, 2003; *Edwards et al.*, 1993] and the relationship that a one meter increase in sea level change equates to a change of −0.008 ‰ in global $\delta^{18}O_{SW}$ values [*Siddall et al.*, 2003]. The estimated $\pm 1\sigma$ uncertainty on the smoothed record is shown by the black bar on the *y* axis. Black triangles on the *x* axis indicate intervals with calibrated radiocarbon dates and their associated error based on mixed samples of the planktonic foraminifera *G. ruber* and *G. sacculifer*.

$\sigma_{combined} = \sigma_{analytical} + \sigma_{calibration}/\sqrt{n}$ (where *n* is the number of points in the smoothing function). We estimate the $\pm 1\sigma$ uncertainty on calculated $\delta^{18}O_{SW}$ values to be ~0.25 ‰ based on the propagation of the $\pm 1\sigma$ errors from the Mg/Ca and $\delta^{18}O$ analyses along with the reported errors from *Anand et al.* [2003] for equation (1), and *Bemis et al.* [1998] for equation (2). Using a variety of methods, prior studies report similar error propagations for the $\delta^{18}O_{SW}$ residuals based on $\delta^{18}O_C$ and Mg/Ca-SSTs in *G. ruber*, ranging from ±0.18 ‰ to ±0.26 ‰ [*Carlson et al.*, 2008; *Lea et al.*, 2000; *Lund and Curry*, 2006; *Oppo et al.*, 2009; *Schmidt et al.*, 2004, 2006; *Weldeab et al.*, 2006]. To calculate the $\pm 1\sigma$ error on the smoothed $\delta^{18}O_{IVF\text{-}SW}$ record on Figures 2c and 5a, we used the following equation: $\sigma = \sigma_{propagated}/\sqrt{n}$ (where *n* is the number of points in the smoothing function).

4. Results

4.1. *Globigerinoides ruber* $\delta^{18}O_C$

[16] The *G. ruber* $\delta^{18}O_C$ record shows an average Holocene value of −1.67 ‰. Based on the raw data, the $\delta^{18}O_C$ record reaches a maximum value of −1.23 ‰ at 7.7 kyr and a minimum value of −2.07 ‰ at 8.0 kyr, with a maximum variability of ~0.8 ‰ (Figure 2a). Throughout the high-resolution section of the record during the early Holocene, there are significant enrichments in $\delta^{18}O$ at ~8.5, 7.7, and 6.6 kyr and depletions at ~8.0, 7.4, 6.8, 6.5, and 6.4 kyr. The lower-resolution mid to late Holocene record shows an enrichment at ~4.3 kyr that is followed within 100 years by an abrupt depletion in $\delta^{18}O$. *Lund and Curry* [2006] measured $\delta^{18}O$ in *G. ruber* from the late Holocene in a core located near JPC 51. Their record showed millennial-scale climate oscillations of about ~0.7 ‰ in oxygen isotope variation during the late Holocene, similar to what we find for the early Holocene. Therefore, oxygen isotope records from the Florida Margin of the Florida Straits derived from

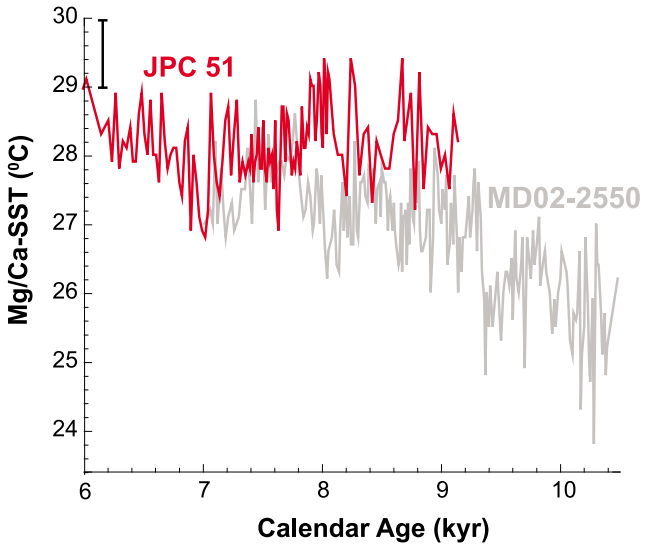

Figure 3. Comparison of the Mg/Ca-SST records from the Florida Straits (JPC 51 in red) and the northern Gulf of Mexico's Orca Basin (MD02–2550 in gray) [*LoDico et al.*, 2006] calculated using the Mg/Ca-SST relationship in *Anand et al.* [2003]. The estimated $\pm 1\sigma$ uncertainty on the JPC 51 SST record is shown by the black bar on the *y* axis. Because the Orca Basin SST record is also based on Mg/Ca ratios in *G. ruber* and has been calibrated using the same Mg/Ca-SST relationship [*Anand et al.*, 2003], the estimated error on this record is assumed to be similar.

G. ruber suggest the presence of persistent millennial-scale climate cycles over the past 10,000 years.

4.2. Mg/Ca-SST

[17] The Mg/Ca-SST record indicates a core top temperature of 27.3°C, in good agreement with the modern average annual SST of ~27.5°C in the Florida Straits [*Locarnini et al.*, 2006] (Figure 2b). The early Holocene section of the record is marked by a warm interval from 8.1 to 7.9 kyr when temperatures reached 29.2°C. Following this warm interval, the record shows a gradual cooling trend lasting ~1 kyr with the coolest temperatures of 27.2°C reached at 7.0 to 6.9 kyr. The high-resolution early Holocene record then shows another warming trend with peak temperatures of just less than 29.0°C reached by 6.5 kyr. The lower-resolution part of the record indicates similar temperature fluctuations in the Florida Straits over the last 6 kyr ranging from ~29°C–27°C.

4.3. Change of $\delta^{18}O_{SW}$

[18] Next, we calculated $\delta^{18}O_{SW}$ change using the Mg/Ca-temperatures and the measured $\delta^{18}O_C$ values in equation (2). Finally, we accounted for global $\delta^{18}O_{SW}$ changes due to Holocene sea level rise as described in section 3.5, thereby calculating a local record of $\delta^{18}O_{IVF\text{-}SW}$ (Figure 2c). The core top $\delta^{18}O_{IVF\text{-}SW}$ value is 0.91 ‰, in good agreement with the estimated modern average $\delta^{18}O_{SW}$ value in the Florida Straits of 0.95 ‰ (calculated using the modern annual mean SSS and the regional SSS:$\delta^{18}O_{SW}$ relationship shown below in equation (3)). During the early-mid Holocene, the record shows three clearly defined cycles with $\delta^{18}O_{IVF\text{-}SW}$ values ranging from 0.6 ‰ to 1.4 ‰, resulting in a maximum amplitude of about 0.8 ‰ across each of these early Holocene events. The three periods of elevated early Holocene $\delta^{18}O_{IVF\text{-}SW}$ values are from 8.3 to 8.0 kyr, 7.6 to 7.4 kyr and 6.6 to 6.3 kyr. In the lower resolution portion of the record, there are two prominent enrichments at 4.2 and 1.8 kyr.

4.4. Conversion of $\delta^{18}O_{IVF\text{-}SW}$ to SSS

[19] Using the modern tropical Atlantic $\delta^{18}O_{SW}$:SSS relationship calculated from regional SSS and $\delta^{18}O_{SW}$ data in the global database of *Schmidt et al.* [1999],

$$\delta^{18}O_{SW}(‰) = 0.26*S(\text{psu}) - 8.44 \quad (3)$$

our core top $\delta^{18}O_{IVF\text{-}SW}$ value corresponds to a salinity of 35.8. This agrees well with the modern average annual salinity of ~36.1 for the Florida Straits [*Antonov et al.*, 2006]. Based on this modern regression, a change of 0.26 ‰ in $\delta^{18}O_{SW}$ is equivalent to a change in SSS of 1.0. Therefore, the calculated $\delta^{18}O_{IVF\text{-}SW}$ values from JPC 51 suggest Holocene SSS changes ranging from 34.4 to 38.2 with an average of 36.2. Given that this range in SSS seems too large for realistic Holocene SSS variability in the Florida Straits, it is likely that the slope of the $\delta^{18}O_{SW}$:SSS relationship must have changed over the Holocene. As discussed in *Lund et al.* [2006], it is also possible that thermocline waters influenced the entire tropical/subtropical $\delta^{18}O_{SW}$:SSS relationship during the Holocene. Because thermocline waters are ventilated at high latitudes, the $\delta^{18}O_{SW}$:SSS slope is steeper (0.5 ‰ per unit salinity change) than the tropical relationship. If this were the case, then $\delta^{18}O_{SW}$ changes of 0.5 ‰ would equate to salinity changes of 1.0, thus reducing our estimated SSS change in JPC 51 to <2.0 across the Holocene.

[20] Based on the results of a coupled GCM modeling study, *Oppo et al.* [2007] found significant tropical hydrologic cycle variability across the Holocene associated with orbital changes in solar insolation. Their results suggest a decrease in water vapor transport across the Central American Isthmus during the mid Holocene associated with a northward shift in the position of the ITCZ and a decrease in the strength of the Pacific easterlies. Because the trade winds transport isotopically depleted water vapor from the Atlantic to the Pacific, modeling results suggest that a decrease in the net water vapor transport across the Central American Isthmus results in a decrease in $\delta^{18}O_{PRECIPITATION}$ values in the western tropical Atlantic during the mid Holocene [*Oppo et al.*, 2007]. More negative $\delta^{18}O_{PRECIPITATION}$ values in the circum-Caribbean region would result in a steeper $\delta^{18}O_{SW}$:SSS relationship, thus reducing the magnitude of SSS change estimated from our $\delta^{18}O_{IVF\text{-}SW}$ record for the early to mid Holocene. Therefore, SSS estimates calculated from our mid to early Holocene $\delta^{18}O_{IVF\text{-}SW}$ record should only be viewed as estimates.

5. Discussion

5.1. Holocene SST Record

[21] Today, water flows more directly from the Yucatan Channel into the Florida Straits during periods of reduced Loop Current penetration [*Lee et al.*, 1995]. Periods of reduced Loop Current penetration also result in the formation of fewer Tortugas eddies [*Lee et al.*, 1995]. This results in a shift in the axis of the Florida Current northward and warmer SSTs at our study site due to an increase in the component of warm Caribbean surface water. Although instrumental data suggests that eddy formation today is stochastic and unrelated to climate forcing [*Maul and Vukovich*, 1993; *Sturges and Leben*, 2000; *Vukovich*, 1988], significant changes in Loop Current penetration and Tortugas eddy formation over the Holocene could impact SSTs at our site. A reconstruction of Loop Current penetration into the Gulf of Mexico based on foraminiferal faunal changes in a core from the northern Gulf of Mexico showed a gradual increase in Loop Current strength from about 9 to 6 kyr, followed by a gradual decrease into the modern [*Poore et al.*, 2004; *Poore et al.*, 2003]. This mid-Holocene peak in reconstructed Loop Current strength at 6 kyr is not reflected as a cooling in our Mg/Ca-SST record from JPC 51 (Figure 2b). Instead, the JPC 51 SST record indicates one of the warmest periods in our record centered at ~6.0 kyr. Therefore, we do not find evidence that SSTs at our study site are significantly influenced by changes in Tortugas eddy formation during the Holocene.

[22] *LoDico et al.* [2006] published a high-resolution (~30 yr sample spacing) SST reconstruction from the northern Gulf of Mexico's Orca Basin spanning from 10.5 to 7.0 kyr based on Mg/Ca ratios in *G. ruber* (white variety). *LoDico et al.* [2006] did not use the reductive cleaning step in their methods. Because the reductive cleaning step in the Mg/Ca cleaning protocol has been shown to lower shell Mg/Ca ratios by 10% [*Pena et al.*, 2005], we decreased their reported Mg/Ca values by 10% to make them more suitable

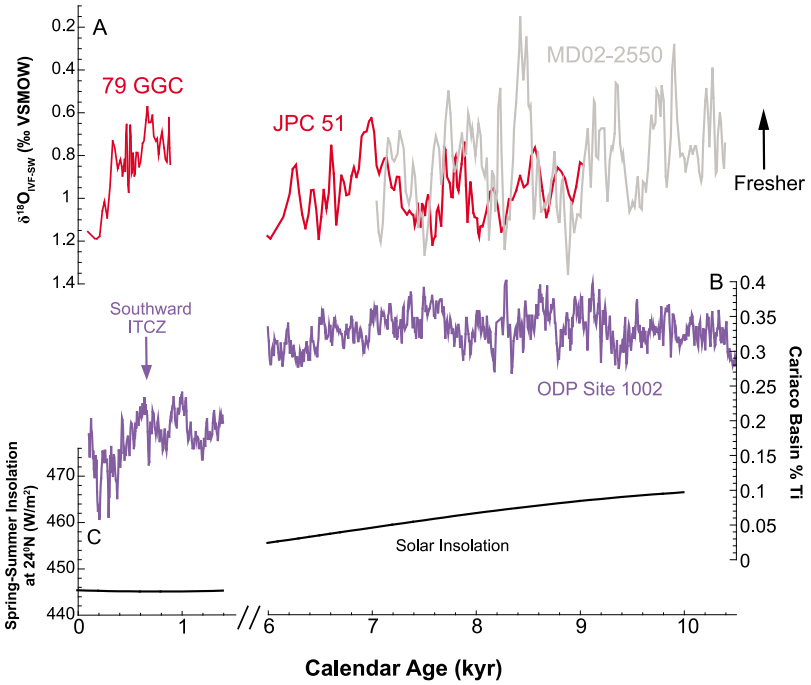

Figure 4. (a) Comparison of $\delta^{18}O_{IVF\text{-}SW}$ records from Florida Straits cores 79 GGC (red, late Holocene) [*Lund and* Curry, 2004] and JPC 51 (red, early Holocene) with the $\delta^{18}O_{IVF\text{-}SW}$ record from Orca Basin core MD02–2550 (gray, early Holocene) [*LoDico et al.*, 2006]. (b) Record of percent titanium in Cariaco Basin core ODP 1002 [*Haug et al.*, 2001], indicating more arid conditions and a southerly shift in the ITCZ during intervals of reduced % Ti values. The % Ti values remain elevated during the early Holocene, suggesting a more permanent northward position of the ITCZ and wetter conditions over northern Venezuela at this time [*Haug et al.*, 2001]. (c) Local spring and summer insolation values at 24°N calculated from *Paillard et al.* [1996].

for comparison to the results in this study. We also updated the age model for the *LoDico et al.* [2006] record by recalibrating their radiocarbon dates using CALIB 6.0 (Figure 3).

[23] The *LoDico et al.* [2006] SST record indicates an abrupt warming at 9.4 kyr, followed by millennial-scale oscillations of ~1.0°C (gray curve on Figure 3). In contrast, the Florida Straits SST record indicates warmer conditions during the early Holocene from 9.2 to 7.8 kyr when the two records overlap. Similar SSTs are then recorded at both sites from 7.8 to 7.3 kyr. While the Florida Straits SST record shows early Holocene centennial-scale SST cycles that are similar in magnitude to those reconstructed for the Orca Basin, the timing of these oscillations is not the same, suggesting unique forcing mechanisms on SSTs at each site.

[24] The greatest difference between the Florida Straits and Orca Basin SST records occurs between ~8.8 to 8.6 kyr and from ~8.2 to 7.8 kyr. It is possible that the different temperature evolution between the two sites is due to the fact that the northern Gulf of Mexico is more directly influenced by continental North American climate, whereas hydrographic conditions in the Florida Straits are more influenced by waters from the western tropical Atlantic [*Schmitz and Richardson*, 1991]. This may explain why the Orca Basin records a cooling after about 8.2 kyr, just as SSTs in the Florida Straits indicate a warming trend over this same interval. The 8.2 kyr event is thought to be the largest climate anomaly of the entire Holocene [*Alley and Agustsdottir*, 2005]. It is possible that the high-latitude cooling associated with the 8.2 kyr event and the proposed reduction in AMOC that lasted several hundred years after the event [*Ellison et al.*, 2006] resulted in cooler surface temperatures over the North American continent, but had less of an impact in the tropical Atlantic. The significant cooling recorded in the Orca Basin after 8.2 kyr most likely reflects the influence of cooler temperatures over continental North America, while the corresponding warmer SSTs in the Florida Straits suggest the tropics may have been less affected by the high-latitude cooling.

5.2. Holocene $\delta^{18}O_{IVF\text{-}SW}$ and Salinity Variability

[25] First, we compare the JPC 51 early Holocene record of $\delta^{18}O_{IVF\text{-}SW}$ with the previously published late Holocene $\delta^{18}O_{IVF\text{-}SW}$ record from Florida Straits core 79 GGC [*Lund and Curry*, 2006] (Figure 4a). Core 79 GGC is located near JPC 51 and the $\delta^{18}O_{IVF\text{-}SW}$ record was calculated using the same methodologies and calibration equations. Comparison of the two records shows that both the early and late Holocene were characterized by similar magnitude $\delta^{18}O_{IVF\text{-}SW}$ oscillations with almost the same average value (the two red curves in Figure 4a). In their study, *Lund and Curry* [2006] observed fresher surface conditions in the Florida Straits during the MWP and saltier surface conditions during the LIA. They argued that the development of elevated $\delta^{18}O_{SW}$ values (and higher SSS) in the Florida Straits during the LIA resulted from increased E/P ratios in the northern

tropical Atlantic associated with a southward shift in the Hadley cell circulation and the ITCZ, as reflected in the percent titanium record from the Cariaco Basin [*Haug et al.*, 2001] (Figure 4b).

[26] In order to determine if meridional shifts in the ITCZ correspond with early Holocene $\delta^{18}O_{IVF\text{-}SW}$ variability, we compare our new JPC 51 record with the Cariaco Basin titanium record (Figures 4a and 4b). The titanium record from the Cariaco Basin was interpreted to suggest that the southern Caribbean was characterized by an enhanced hydrologic cycle during the early Holocene [*Haug et al.*, 2001], a period marked by increased spring-summer insolation when precession was at a maximum in the northern tropics (Figure 4c). Ostracod $\delta^{18}O$ records from Haitian lake cores also indicate wetter conditions in the northern Caribbean during the early Holocene [*Hodell et al.*, 1991]. Therefore, rainfall amounts in the circum-Caribbean region were most likely at a maximum during the early Holocene, probably reflecting a more intense summer ITCZ located farther to the north. Although the JPC 51 record indicates large $\delta^{18}O_{IVF\text{-}SW}$ oscillations during the early Holocene that are similar in magnitude with those recorded for the MWP – LIA transition of the late Holocene [79 GGC record on Figure 4a from *Lund and Curry*, 2006], the JPC 51 $\delta^{18}O_{IVF\text{-}SW}$ oscillations from 9.2 to 6.2 kyr do not correlate with changes in the Cariaco Basin percent titanium record during this interval ($R = 0.20$, $R^2 = 0.04$). Therefore, early Holocene $\delta^{18}O_{IVF\text{-}SW}$ cycles in the Florida Straits cannot simply be explained by meridional shifts in the ITCZ.

[27] Second, we compare our early Holocene $\delta^{18}O_{IVF\text{-}SW}$ record with a similar resolution $\delta^{18}O_{IVF\text{-}SW}$ reconstruction from the northern Gulf of Mexico's Orca Basin (gray curve on Figure 4a) [*LoDico et al.*, 2006]. In order to directly compare the JPC 51 $\delta^{18}O_{IVF\text{-}SW}$ reconstruction with the Orca Basin record, we recalculated their data using equations (1) and (2) and then corrected the resulting $\delta^{18}O_{SW}$ values for continental ice volume variability using the same global $\delta^{18}O_{SW}$ we used to calculate our $\delta^{18}O_{IVF\text{-}SW}$ values. Overall, the calculated $\delta^{18}O_{IVF\text{-}SW}$ values from both locations show similar scale oscillations, most notably between 9.2 to 8.6 kyr and 7.8 to 7.1 kyr. However, the Orca Basin $\delta^{18}O_{IVF\text{-}SW}$ record indicates two significant freshening events between 8.4 and 8.0 kyr that are not recorded in the JPC 51 record. Just as the SST comparison between the Orca Basin and the Florida Straits indicates the development of a steep temperature gradient across the Gulf of Mexico after the 8.2 kyr event (Figure 3), the $\delta^{18}O_{IVF\text{-}SW}$ comparison suggests large differences in SSS between the two sites as well. The cool, fresh conditions in the northern Gulf of Mexico associated with the 8.2 kyr event apparently did not extend into the Florida Straits.

[28] Several studies suggest the primary driver of early Holocene climate change on centennial to millennial time scales is variability in solar forcing [*Bond et al.*, 1997, 2001; *Lund and Curry*, 2004; *Roth and Reijmer*, 2005]. *Bond et al.* [2001] found increases in ice rafted debris (IRD) in North Atlantic sediments about every 1500 years and showed that intervals associated with increased IRD correspond to periods of elevated ^{14}C production in the atmosphere. More ^{14}C is produced in the atmosphere during periods of reduced solar winds, so periods of increased IRD correspond to intervals of reduced solar forcing (Figures 5d, 5e, and 5f).

[29] In addition, several ocean-atmosphere modeling studies point to the tropical Pacific as playing a major role in driving sub orbital-scale climate variability [*Bush and Philander*, 1998; *Cane and Clement*, 1999; *Cane*, 1998; *Clement and Cane*, 1999; *Kukla et al.*, 2002]. These studies suggest that the El Niño-Southern Oscillation (ENSO) is controlled by changes in seasonal cycle forcing at the equator, correlating periods of reduced summer irradiance in the tropical Pacific (decreased seasonality) with stronger El Niño forcing. According to the Zebiak-Cane model of ENSO dynamics, relatively small changes in total irradiance can cause the background state of the tropical Pacific to oscillate between El Niño/La Niña states [*Mann et al.*, 2005].

[30] A recent study by *Marchitto et al.* [2010] showed that changes in solar forcing during the early Holocene had a large impact on ENSO variability in the eastern equatorial Pacific (EEP). *Marchitto et al.* [2010] reconstructed Holocene SST anomalies off the coast of Baja California Sur, Mexico in the Soledad Basin using Mg/Ca ratios in the planktonic foraminifera *Globigerina bulloides. Marchitto et al.* [2010] first smoothed their Mg/Ca-SST anomaly record using a 250-year running mean to remove high-frequency climate variability that cannot be reliably correlated with other proxy records (Figure 5b). They then smoothed the Holocene records of ^{14}C [*Reimer et al.*, 2004] and ^{10}Be production [*Finkel and Nishiizumi*, 1997; *Vonmoos et al.*, 2006] using the same 250-year running mean and then removed the long-term drift in the nuclide records resulting from slow variations in the Earth's geomagnetic field [*Wagner et al.*, 2000] by performing a high pass filter at 1/1800-year (Figures 5e and 5f). This same high pass filter was used by *Bond et al.* [2001] to generate their stacked IRD record shown on Figure 5d. As a result, *Marchitto et al.* [2010] identified five warm intervals between 11 to 7 kyr (more El Niño-like conditions) separated by roughly 1 kyr that corresponded to periods of increased ^{14}C and ^{10}Be production (times of reduced solar activity). *Marchitto et al.* [2010] argued that centennial-scale changes in solar output resulted in stronger El Niño forcing in the tropical Pacific during times of reduced solar output. Comparison of the Soledad Basin SST record with *Bond et al.*'s [2001] IRD record also suggests a strong correlation between cool periods in the North Atlantic and more El Niño-like conditions in the EEP. Previous research also showed that the Asian monsoon system weakens during periods of reduced solar output (Figure 5c) [*Wang et al.*, 2005]. Comparison of the Dongge Cave (southern China) oxygen isotope record with the Soledad Basin SST anomaly record shows that a weaker Asian monsoon correlates with stronger El Niño forcing in the tropical Pacific [*Marchitto et al.*, 2010].

[31] In order to determine how early Holocene ENSO variability in the Pacific may have affected hydrologic changes in the western tropical Atlantic, we compare the Soledad Basin Mg/Ca-SST anomaly record (Figure 5b) with our new JPC 51 $\delta^{18}O_{IVF\text{-}SW}$ record from the Florida Straits (also smoothed with a 250-year running mean) (Figure 5a). As warm anomalies developed in the EEP associated with a shift to more permanent El Niño-like conditions, $\delta^{18}O_{IVF\text{-}SW}$ values in the Florida Straits increased, suggesting an increase in tropical Atlantic E/P ratios and more arid

conditions. The strong correlation between these two records suggests that ENSO variability in the EEP is linked to hydrologic changes in the western tropical Atlantic. It is not surprising that more permanent El Niño-like conditions in the EEP are associated with a more arid circum-Caribbean climate. El Niño events are associated with reduced rainfall, warmer SSTs, and weaker trade winds in the western tropical North Atlantic [*Alexander and Scott*, 2002; *Alexander et al.*, 2002; *Giannini et al.*, 2001a, 2001b; *Poveda and Mesa*, 1997]. Based on coupled ocean-atmosphere general circulation model results [*Schmittner and Clement*, 2002; *Schmittner et al.*, 2000] and reanalysis of two historical data sets [*Schmittner et al.*, 2000], El Niño events may even result in enhanced water vapor transport out of the tropical Atlantic.

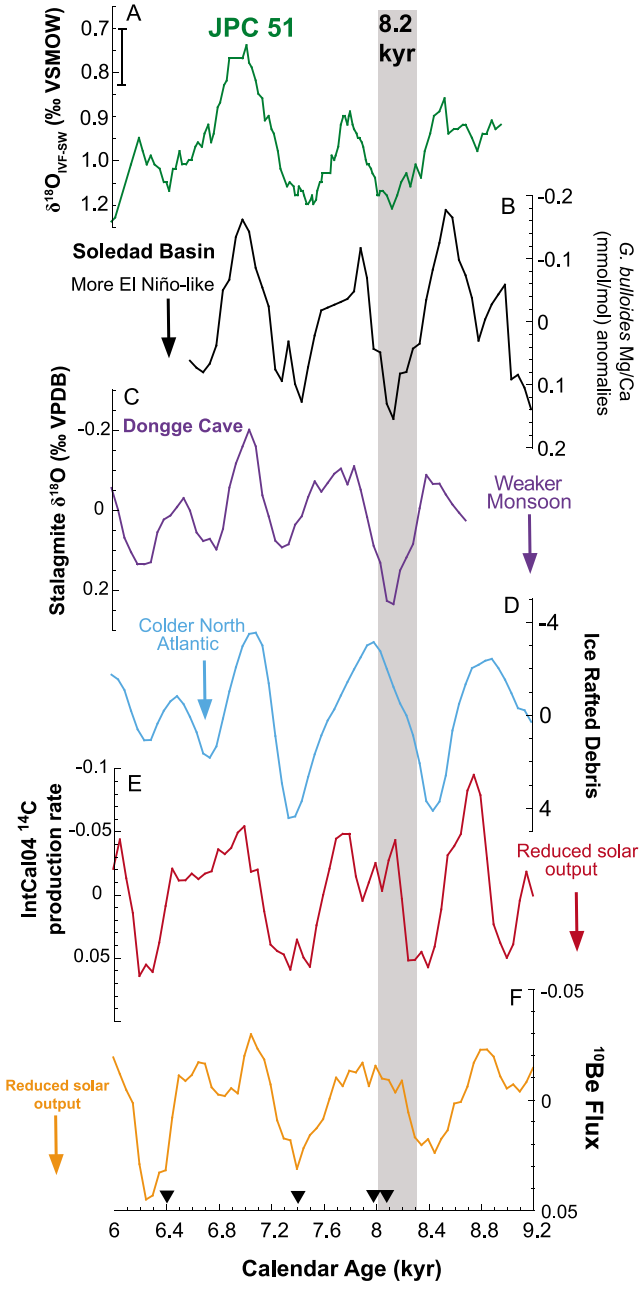

[32] Furthermore, proxies for solar variability also covary with the JPC 51 $\delta^{18}O_{IVF-SW}$ record. Intervals of increased ^{14}C and ^{10}Be production (Figures 5e and 5f) correspond to intervals of more positive $\delta^{18}O_{IVF-SW}$ values in the Florida Straits. In addition, periods of increased IRD also correlate to elevated $\delta^{18}O_{IVF-SW}$ values in the Florida Straits, indicating that cool periods in the high-latitude North Atlantic are associated with drier conditions in the tropical North Atlantic during the early Holocene. Finally, drier conditions in the Florida Straits correlate to increased oxygen isotope values in speleothem records from Dongge Cave, indicating a weakening of the Asian monsoon (Figure 5c). Taken together, correlations between the Florida Straits $\delta^{18}O_{IVF-SW}$ record, the Soledad Basin Mg/Ca-SST anomaly record from the EEP, IRD changes in the North Atlantic and variations in the strength of the Asian monsoon all suggest dramatic reorganizations of atmospheric circulation patterns around the globe driven by variability in solar forcing during the early Holocene.

[33] Although it is thought that increased solar irradiance generates a stronger interplanetary magnetic field that shields Earth from the cosmic rays that form ^{14}C and ^{10}Be in the atmosphere, this relationship is not well understood over long time periods. Atmospheric ^{14}C content can also be influenced by the global carbon cycle [*Hughen et al.*, 1998] and local climate variability can affect the ^{10}Be flux to ice sheets [*Finkel and Nishiizumi*, 1997]. Furthermore, the

Figure 5. (a) Early Holocene $\delta^{18}O_{IVF-SW}$ from JPC 51 smoothed with a 250-year running mean. The estimated $\pm 1\sigma$ uncertainty on the smoothed record is shown by the black bar on the *y* axis. (b) Planktonic foraminiferal Mg/Ca-SST anomalies from the Soledad Basin (Baja California Sur, Mexico) smoothed with a 250-year running mean [*Marchitto et al.*, 2010]. SST changes in the Soledad Basin are interpreted to reflect shifts in the mean ENSO state in the tropical Pacific, with warmer temperatures associated with periods characterized by more permanent El Niño-like conditions [*Marchitto et al.*, 2010]. The age model for the Soledad Basin record is based on four calibrated radiocarbon dates across this interval. (c) Stalagmite $\delta^{18}O$ record from Dongge Cave (southern China) indicating changes in the strength of the Asian monsoon [*Wang et al.*, 2005]. The age model for the Dongge Cave record is based on absolute-dated U-Th ages. (d) Stacked ice-rafted debris record from the North Atlantic [*Bond et al.*, 2001] indicating times of cooler North Atlantic climate when IRD was greater. (e) IntCal04 ^{14}C production rate based on tree ring-derived $\Delta^{14}C$ [*Reimer et al.*, 2004] and (f) ^{10}Be flux from the GRIP-GISP2 ice cores [*Finkel and Nishiizumi*, 1997; *Vonmoos et al.*, 2006]. Note the development of more El Niño-like conditions in the eastern equatorial Pacific and saltier conditions in the Florida Straits during times of reduced solar output. Also indicated with the shaded gray bar is the 8.2 kyr event. Note the 8.2 kyr event occurs at a time of increasing solar activity, but that SSS remained elevated in the Florida Straits and SSTs in the EEP remain warm. This suggests the cool conditions in the North Atlantic caused by freshwater forcing prevented the tropics from responding to the increase in solar activity at this time. Black triangles on the *x* axis indicate intervals with calibrated radiocarbon dates in JPC 51 (see Table 1 for associated errors on the radiocarbon dates).

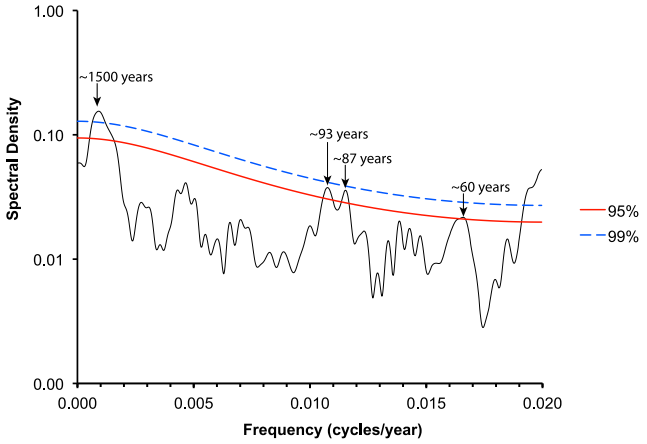

Figure 6. Multitaper spectral analysis results of the high-resolution JPC 51 $\delta^{18}O_{IVF\text{-}SW}$ record from from 9.1 to 6.2 kyr showing high spectral power above the 95% confidence level at periods of ~1500, 93, 87 and 60 years.

atmospheric concentration of both nuclides is influenced by long-term changes in Earth's geomagnetic field. Nevertheless, *Marchitto et al.* [2010] argued that long-term changes in Earth's geomagnetic field can be filtered from each nuclide record using a high-pass filter. Therefore, shared variability between the high-pass filtered ^{14}C and ^{10}Be records shown on Figure 5 (filtered data from *Marchitto et al.* [2010] suggests that changes in solar irradiance are the most likely cause [*Marchitto et al.*, 2010].

[34] Although we cannot determine whether forcing from the tropical Pacific (ENSO) or the high-latitude North Atlantic had the strongest impact on the tropical Atlantic hydrologic cycle, the strong cooling in the North Atlantic associated with the 8.2 kyr event seems to have locked the tropical hydrologic cycle into a 'cold phase.' During the 8.2 kyr event, the final drainage of large pro-glacial lakes into the North Atlantic is thought to have resulted in a meltwater-induced reduction in AMOC that caused widespread cooling in the circum-Atlantic region [*Alley and Agustsdottir*, 2005; *Barber et al.*, 1999; *Clarke et al.*, 2004; *Ellison et al.*, 2006]. Although the JPC 51 $\delta^{18}O_{IVF\text{-}SW}$ record covaries with changes in solar forcing across two complete cycles (~7.4 to 6.2 kyr and 8.0 to 7.4 kyr), the correlation decreases during the interval around the 8.2 kyr event (gray bar on Figure 5). Although the IRD record does not indicate cold conditions in the North Atlantic during the 8.2 kyr event, this record is relatively low-resolution and may not fully resolve the 8.2 kyr event. Nevertheless, several other proxy studies indicate the high-latitude North Atlantic remained cold during the 8.2 kyr event [*Alley and Agustsdottir*, 2005; *Barber et al.*, 1999; *Clarke et al.*, 2004; *Ellison et al.*, 2006]. Because the 8.2 kyr event was forced by an internal driver rather than by external changes in solar variability, it is not surprising that the JPC 51 $\delta^{18}O_{IVF\text{-}SW}$ record does not match the solar output proxies at this time. Instead, the JPC 51 $\delta^{18}O_{IVF\text{-}SW}$ record shows a much better correlation with the Soledad Basin SST-anomalies and the Dongge Cave record during the 8.2 kyr event because these records probably reflect a teleconnected response to the high-latitude cooling. The 8.2 kyr event occurred at a time of increasing solar activity, but SSS remained elevated in the Florida Straits, SST's in the EEP remained warm and the Asian monsoon remained weak. This suggests the cool conditions in the North Atlantic caused by freshwater forcing prevented the tropics from responding to the increase in solar activity at this time.

[35] *Saenger et al.* [2009] used a coupled GCM to isolate the impact of high-latitude cooling on the tropical Atlantic hydrologic cycle. Their results show that a 2°C cooling in the North Atlantic results in increased wind stress and negative precipitation anomalies in the tropical North Atlantic. The high-latitude cooling increases the strength of the northeast trade winds, resulting in increased evaporation rates in the tropical Atlantic. Therefore, the elevated $\delta^{18}O_{IVF\text{-}SW}$ values in JPC 51 associated with increased North Atlantic IRD (and a cooler North Atlantic) are also consistent with this high-to-low latitude climate teleconnection, reflecting increased E/P ratios in the Florida Straits during periods of high-latitude cooling.

5.3. Spectral Analysis

[36] To determine the frequency of sub-orbital cycles in our high-resolution early Holocene $\delta^{18}O_{IVF\text{-}SW}$ record, we performed multitaper spectral analysis [*Ghil et al.*, 2002] on our record from 9.1 to 6.2 kyr using a 25-year interpolation of the data (the average sampling resolution for our early Holocene record is 25 years) (Figure 6). The results of the spectral analysis indicate strong spectral power above the 95% confidence level at periodicities of ~1,500, 93, 87 and 60-years. Spectral power at the 1500-year period suggests a strong correlation between solar-driven Bond cycles and hydrologic cycle variability in the Florida Straits. Nevertheless, the length of our record limits our confidence in the peak at 1500 years. Although uncertainty in our age model (up to 194 years during the early Holocene) also limits our confidence in the higher frequency peaks, it is worth noting that spectral power at the 87-year period is common in proxies forced by solar variability, possibly reflecting an influence of the Gleissberg solar cycle [*Peristykh and Damon*, 2003]. Spectral power at the 60-year period may reveal a connection between SSS variability in the Florida Straits and the Atlantic Multidecadal Oscillation (AMO) (30–80 year period) [*Dima and Lohmann*, 2007], which some modeling studies suggest is the result of high-frequency AMOC variability during the Holocene [*Delworth and Mann*, 2000; *Enfield et al.*, 2001; *Heslop and Paul*, 2011]. *Knight et al.* [2006] showed that the warm AMO phase is associated with a northward displacement of the ITCZ over the tropical Atlantic, suggesting a possible influence of the AMO on the tropical Atlantic hydrologic cycle.

6. Conclusions

[37] Our new Mg/Ca-SST record from the Florida Straits indicates only a small (~0.8°C) cooling trend through the Holocene. While the Florida Straits record shows early Holocene centennial-scale SST cycles that are similar in magnitude to those previously reconstructed for the northern Gulf of Mexico in the Orca Basin over the same time interval, the timing of these oscillations is not the same. The greatest difference between the Florida Straits and Orca Basin SST records occurs from ~8.8 to 8.6 kyr and from ~8.2 to 7.8 kyr. We conclude that the contrasting

temperature evolution between the two sites is due to the fact that the northern Gulf of Mexico is more directly influenced by continental North American climate, whereas hydrographic conditions in the Florida Straits are more influenced by the waters from the western tropical Atlantic traveling through the Caribbean and Yucatan Channel to our core site.

[38] After correcting our calculated $\delta^{18}O_{SW}$ record for global changes in $\delta^{18}O_{SW}$ due to continental ice volume variability, the $\delta^{18}O_{IVF\text{-}SW}$ record from the Florida Straits reveals millennial-scale oscillations on the order of 0.8 ‰. Comparison of our early Holocene $\delta^{18}O_{IVF\text{-}SW}$ record with the late Holocene $\delta^{18}O_{IVF\text{-}SW}$ reconstruction from the same location in the Florida Straits [*Lund and Curry*, 2006] shows that both periods were characterized by similar magnitude $\delta^{18}O_{IVF\text{-}SW}$ variability. The periods of increased SSS (more positive $\delta^{18}O_{IVF\text{-}SW}$ values) during the early Holocene are associated with North Atlantic cooling and the development of El Niño-like conditions in the EEP. As solar output decreased on millennial time scales during the early Holocene, proxy records from the EEP suggest the development of more permanent El Niño-like conditions in the tropical Pacific, and Chinese speleothem records indicate intervals of a weakened Asian monsoon. At the same time, these events are associated with elevated SSS in the Florida Straits, providing evidence for a dramatic reorganization of atmospheric circulation patterns around the globe driven by Holocene changes in solar output.

[39] Finally, we show that the strong cooling in the North Atlantic associated with the 8.2 kyr event seems to have locked the tropical hydrologic cycle into a 'cold phase.' Because the 8.2 kyr event was forced by an internal driver rather than by changes in solar variability, the JPC 51 $\delta^{18}O_{IVF\text{-}SW}$ record reflects a teleconnected response to the high-latitude cooling at 8.2 kyr. Although nuclide records suggest solar irradiance was increasing at the start of the 8.2 kyr event, SSS remained elevated in the Florida Straits for several hundred years after the meltwater-induced collapse of AMOC. This suggests a strong coupling between high-latitude North Atlantic climate and the tropical Atlantic hydrologic cycle.

[40] **Acknowledgments.** We thank the National Science Foundation (grant OCE-0823498 (MWS)) for supporting this research. We also thank Jennifer Hertzberg for input on the manuscript and for technical help.

References

Alexander, M., and J. Scott (2002), The influence of ENSO on air-sea interaction in the Atlantic, *Geophys. Res. Lett.*, *29*(14), 1701, doi:10.1029/2001GL014347.

Alexander, M. A., I. Blade, M. Newman, J. R. Lanzante, N. C. Lau, and J. D. Scott (2002), The atmospheric bridge: The influence of ENSO teleconnections on air-sea interaction over the global oceans, *J. Clim.*, *15*(16), 2205–2231, doi:10.1175/1520-0442(2002)015<2205:TABTIO>2.0.CO;2.

Alley, R. B., and A. M. Agustsdottir (2005), The 8 k event: Cause and consequences of a major Holocene abrupt climate change, *Quat. Sci. Rev.*, *24*(10–11), 1123–1149, doi:10.1016/j.quascirev.2004.12.004.

Anand, P., H. Elderfield, and M. H. Conte (2003), Calibration of Mg/Ca thermometry in planktonic foraminifera from a sediment trap time series, *Paleoceanography*, *18*(2), 1050, doi:10.1029/2002PA000846.

Antonov, J. I., R. A. Locarnini, T. P. Boyer, A. V. Mishonov, and H. E. Garcia (2006), *World Ocean Atlas 2005*, vol. 2 , *Salinity*, *NOAA Atlas NESDIS*, vol. 62, edited by S. Levitus, 182 pp., NOAA, Silver Spring, Md.

Antonov, J. I., D. Seidov, T. P. Boyer, R. A. Locarnini, A. V. Mishonov, H. E. Garcia, O. K. Baranova, M. M. Zweng, and D. R. Johnson (2010), *World Ocean Atlas 2009*, vol. 2, *Salinity*, *NOAA Atlas NESDIS*, vol. 69, edited by S. Levitus, 184 pp., NOAA, Silver Spring, Md.

Arbuszewski, J., P. deMenocal, A. Kaplan, and E. Farmer (2010), On the Fidelity of Shell-Derived δ18Oseawater Estimates, *Earth Planet. Sci. Lett.*, *300*, 185–196, doi:10.1016/j.epsl.2010.10.035.

Barber, D. C., et al. (1999), Forcing of the cold event of 8,200 years ago by catastrophic drainage of Laurentide lakes, *Nature*, *400*(6742), 344–348, doi:10.1038/22504.

Bard, E., B. Hamelin, and R. G. Fairbanks (1990), U-Th ages obtained by mass spectrometry in corals from Barbados: Sea level during the past 130,000 years, *Nature*, *346*, 456–458, doi:10.1038/346456a0.

Bemis, B. E., H. J. Spero, J. Bijima, and D. W. Lea (1998), Reevaluation of the oxygen isotopic composition of planktonic foraminifera: Experimental results and revised paleotemperature equations, *Paleoceanography*, *13*(2), 150–160, doi:10.1029/98PA00070.

Bond, G., W. Showers, M. Cheseby, R. Lotti, I. Hajdas, and G. Bonani (1997), A pervasive millennial-scale cycle in North Atlantic Holocene and glacial climates, *Science*, *278*, 1257–1266, doi:10.1126/science.278.5341.1257.

Bond, G., B. Kromer, J. Beer, R. Muscheler, M. N. Evans, W. Showers, S. Hoffmann, R. Lotti-Bond, I. Hajdas, and G. Bonani (2001), Persistent solar influence on north Atlantic climate during the Holocene, *Science*, *294*(5549), 2130–2136, doi:10.1126/science.1065680.

Brunner, C. A. (1982), Paleo-oceanography of surface waters in the Gulf of Mexico during the Late Quaternary, *Quat. Res.*, *17*(1), 105–119, doi:10.1016/0033-5894(82)90048-5.

Bush, A. G., and S. H. Philander (1998), The role of ocean–atmosphere interactions in tropical cooling during the last glacial maximum, *Science*, *279*, 1341–1344, doi:10.1126/science.279.5355.1341.

Cane, M. A. (1998), A role for the Tropical Pacific, *Science*, *282*, 59–61, doi:10.1126/science.282.5386.59.

Cane, M., and A. C. Clement (1999), A role for the tropical Pacific coupled ocean–atmosphere system on Milankovich and millennial timescales Part II: Global impacts, in *Mechanisms of Global Climate Change at Millennial Time Scales*, edited by P. U. Clark, R. S. Webb, and L. D. Keigwin, pp. 373–383, AGU, Washington, D. C., doi:10.1029/GM112p0373.

Carlson, A. E., D. W. Oppo, R. E. Came, A. N. LeGrande, L. D. Keigwin, and W. B. Curry (2008), Subtropical Atlantic salinity variability and Atlantic meridional circulation during the last deglaciation, *Geology*, *36*(12), 991–994, doi:10.1130/G25080A.1.

Clarke, G. K. C., D. W. Leverington, J. T. Teller, and A. S. Dyke (2004), Paleohydraulics of the last outburst flood from glacial Lake Agassiz and the 8200 BP cold event, *Quat. Sci. Rev.*, *23*(3–4), 389–407, doi:10.1016/j.quascirev.2003.06.004.

Clement, A. C., and M. Cane (1999), A role for the Tropical Pacific coupled ocean–atmosphere system on Milankovitch and millennial timescales. Part I: A modeling study of Tropical Pacific variability, in *Mechanisms of Global Climate Change at Millennial Time Scales*, edited by P. U. Clark, R. S. Webb, and L. D. Keigwin, pp. 363–371, AGU, Washington, D. C., doi:10.1029/GM112p0363.

Cutler, K. B., R. L. Edwards, F. W. Taylor, H. Cheng, J. Adkins, C. D. Gallup, P. M. Cutler, G. S. Burr, and A. L. Bloom (2003), Rapid sea-level fall and deep-ocean temperature change since the last interglacial period, *Earth Planet. Sci. Lett.*, *206*(3–4), 253–271, doi:10.1016/S0012-821X(02)01107-X.

Dekens, P. S., D. W. Lea, D. K. Pak, and H. J. Spero (2002), Core top calibration of Mg/Ca in tropical foraminifera: Refining paleotemperature estimation, *Geochem. Geophys. Geosyst.*, *3*(4), 1022, doi:10.1029/2001GC000200.

Delworth, T., and M. E. Mann (2000), Observed and simulated multidecadal variability in the Northern Hemisphere, *Clim. Dyn.*, *16*, 661–676, doi:10.1007/s003820000075.

deMenocal, P., J. Ortiz, T. P. Guilderson, and M. Sarnthein (2000), Coherent high- and low-latitude climate variability during the Holocene warm period, *Science*, *288*, 2198–2202, doi:10.1126/science.288.5474.2198.

Dima, M., and G. Lohmann (2007), A hemispheric mechanism for the Atantic multidecadal oscillation, *J. Clim.*, *20*(11), 2706–2719, doi:10.1175/JCLI4174.1.

Edwards, R., J. Warren Beck, G. S. Burr, D. J. Donahue, M. A. Chappell, A. L. Bloom, E. R. M. Druffel, and F. W. Taylor (1993), A large drop in atmospheric $^{14}C/^{12}C$ and reduced melting in the Younger Dryas, documented with ^{230}Th ages of corals, *Science*, *260*(5110), 962–968, doi:10.1126/science.260.5110.962.

Ellison, C. R. W., M. R. Chapman, and I. R. Hall (2006), Surface and deep ocean interactions during the cold climate event 8200 years ago, *Science*, *312*(5782), 1929–1932, doi:10.1126/science.1127213.

Enfield, D. B., A. M. Mestas-Nunez, and P. J. Trimble (2001), The Atlantic multidecadal oscillation and its relation to rainfall and river flows in the continental US, *Geophys. Res. Lett.*, *28*(10), 2077–2080, doi:10.1029/2000GL012745.

Fairbanks, R. G., C. D. Charles, and J. D. Wright (1992), Origin of global meltwater pulses, in *Radiocarbon After Four Decades*, edited by R. E. Taylor, pp. 473–500, Springer, New York.

Finkel, R. C., and K. Nishiizumi (1997), Beryllium 10 concentrations in the Greenland Ice Sheet Project 2 ice core from 3–40 ka, *J. Geophys. Res.*, *102*(C12), 26,699–26,706, doi:10.1029/97JC01282.

Fratantoni, P. S., T. N. Lee, G. P. Podesta, and F. Muller-Karger (1998), The influence of Loop Current perturbations on the formation and evolution of Tortugas eddies in the southern Straits of Florida, *J. Geophys. Res.*, *103*, 24,759–24,779, doi:10.1029/98JC02147.

Ghil, M., et al. (2002), Advanced spectral methods for climatic time series, *Rev. Geophys.*, *40*(1), 1003, doi:10.1029/2000RG000092.

Giannini, A., M. A. Cane, and Y. Kushnir (2001a), Interdecadal changes in the ENSO teleconnection to the Caribbean region and the North Atlantic oscillation, *J. Clim.*, *14*(13), 2867–2879, doi:10.1175/1520-0442(2001)014<2867:ICITET>2.0.CO;2.

Giannini, A., J. C. H. Chiang, M. A. Cane, Y. Kushnir, and R. Seager (2001b), The ENSO teleconnection to the tropical Atlantic Ocean: Contributions of the remote and local SSTs to rainfall variability in the tropical Americas, *J. Clim.*, *14*(24), 4530–4544, doi:10.1175/1520-0442(2001)014<4530:TETTTT>2.0.CO;2.

Haug, G. H., K. A. Hughen, D. M. Sigman, L. C. Peterson, and U. Röhl (2001), Southward migration of the intertropical convergence zone through the Holocene, *Science*, *293*(5533), 1304–1308, doi:10.1126/science.1059725.

Heslop, D., and A. Paul (2011), Can oceanic paleothermometers reconstruct the Atlantic multidecadal oscillation?, *Clim. Past*, *7*, 151–159, doi:10.5194/cp-7-151-2011.

Hodell, D. A., J. H. Curtis, G. A. Jones, A. Higueragundy, M. Brenner, M. W. Binford, and K. T. Dorsey (1991), Reconstruction of Caribbean climate change over the past 10,500 years, *Nature*, *352*(6338), 790–793, doi:10.1038/352790a0.

Hughen, K. A., et al. (1998), Deglacial changes in ocean circulation from an extended radiocarbon calibration, *Nature*, *391*, 65–68, doi:10.1038/34150.

Knight, J. R., C. K. Folland, and A. A. Scaife (2006), Climate impacts of the Atlantic Multidecadal Oscillation, *Geophys. Res. Lett.*, *33*, L17706, doi:10.1029/2006GL026242.

Kukla, G., A. C. Clement, M. Cane, J. Gavin, and S. Zebiak (2002), Last interglacial and early glacial ENSO, *Quat. Res.*, *58*, 27–31, doi:10.1006/qres.2002.2327.

Lea, D. W., and P. A. Martin (1996), A rapid mass spectrometric method for the simultaneous analysis of barium, cadmium, and strontium in foraminifera shells, *Geochim. Cosmochim. Acta*, *60*(16), 3143–3149, doi:10.1016/0016-7037(96)00184-6.

Lea, D. W., D. K. Pak, and H. J. Spero (2000), Climate impact of late Quaternary equatorial Pacific sea surface temperature variations, *Science*, *289*, 1719–1724, doi:10.1126/science.289.5485.1719.

Lee, T. N., K. Leaman, E. Williams, T. Berger, and L. Atkinson (1995), Florida Current meanders and gyre formation in the southern Straits of Florida, *J. Geophys. Res.*, *100*(C5), 8607–8620, doi:10.1029/94JC02795.

Locarnini, R. A., A. V. Mishonov, J. I. Antonov, T. P. Boyer, and H. E. Garcia (2006), *World Ocean Atlas 2005*, vol. 1 , *Temperature*, *NOAA Atlas NESDIS*, vol. 61, edited by S. Levitus, 182 pp., NOAA, Silver Spring, Md.

LoDico, J. M., B. P. Flower, and T. M. Quinn (2006), Subcentennial-scale climatic and hydrologic variability in the Gulf of Mexico during the early Holocene, *Paleoceanography*, *21*, PA3015, doi:10.1029/2005PA001243.

Lund, D. C., and W. B. Curry (2004), Late holocene variability in Florida current surface density: Patterns and possible causes, *Paleoceanography*, *19*, PA4001, doi:10.1029/2004PA001008.

Lund, D. C., and W. Curry (2006), Florida Current surface temperature and salinity variability during the last millennium, *Paleoceanography*, *21*, PA2009, doi:10.1029/2005PA001218.

Lund, D. C., J. Lynch-Stieglitz, and W. B. Curry (2006), Gulf Stream density structure and transport during the past millennium, *Nature*, *444*(7119), 601–604, doi:10.1038/nature05277.

Lynch-Stieglitz, J., W. B. Curry, and N. Slowey (1999), A geostrophic transport estimate for the Florida Current from the oxygen isotope composition of benthic foraminifera, *Paleoceanography*, *14*(3), 360–373, doi:10.1029/1999PA900001.

Mann, M. E., M. A. Cane, S. E. Zebiak, and A. Clement (2005), Volcanic and solar forcing of the tropical Pacific over the past 1000 years, *J. Clim.*, *18*(3), 447–456, doi:10.1175/JCLI-3276.1.

Marchitto, T. M., R. Muscheler, J. D. Ortiz, J. D. Carriquiry, and A. van Geen (2010), Dynamical response of the tropical Pacific Ocean to solar forcing during the early Holocene, *Science*, *330*(6009), 1378–1381, doi:10.1126/science.1194887.

Maul, G. A., and F. M. Vukovich (1993), The relationship between variations in the Gulf of Mexico Loop Current and Straits of Florida volume transport, *J. Phys. Oceanogr.*, *23*(5), 785–796, doi:10.1175/1520-0485(1993)023<0785:TRBVIT>2.0.CO;2.

Murphy, S. J., H. E. Hurlburt, and J. J. O'Brien (1999), The connectivity of eddy variability in the Caribbean Sea, the Gulf of Mexico, and the Atlantic Ocean, *J. Geophys. Res.*, *104*(C1), 1431–1453, doi:10.1029/1998JC900010.

Nürnberg, D., J. Bijma, and C. Hemleben (1996), Assessing the reliability of magnesium in foraminiferal calcite as a proxy for water mass temperatures, *Geochim. Cosmochim. Acta*, *60*(5), 803–814, doi:10.1016/0016-7037(95)00446-7.

Oppo, D. W., G. A. Schmidt, and A. N. LeGrande (2007), Seawater isotope constraints on tropical hydrology during the Holocene, *Geophys. Res. Lett.*, *34*, L13701, doi:10.1029/2007GL030017.

Oppo, D. W., Y. Rosenthal, and B. K. Linsley (2009), 2,000-year-long temperature and hydrology reconstructions from the Indo-Pacific warm pool, *Nature*, *460*(7259), 1113–1116, doi:10.1038/nature08233.

Paillard, D., L. Labeyrie, and P. Yiou (1996), Macintosh Program performs time-series analysis, *Eos Trans. AGU*, *77*(39), 379, doi:10.1029/96EO00259.

Pena, L. D., E. Calvo, I. Cacho, S. Eggins, and C. Pelejero (2005), Identification and removal of Mn-Mg-rich contaminant phases on foraminiferal tests: Implications for Mg/Ca past temperature reconstructions, *Geochem. Geophys. Geosyst.*, *6*, Q09P02, doi:10.1029/2005GC000930.

Peristykh, A. N., and P. E. Damon (2003), Persistence of the Gleissberg 88-year solar cycle over the last 12,000 years: Evidence from cosmogenic isotopes, *J. Geophys. Res.*, *108*(A1), 1003, doi:10.1029/2002JA009390.

Poore, R. Z., H. J. Dowsett, S. Verardo, and T. M. Quinn (2003), Millennial- to century-scale variability in Gulf of Mexico Holocene climate records, *Paleoceanography*, *18*(2), 1048, doi:10.1029/2002PA000868.

Poore, R. Z., T. M. Quinn, and S. Verardo (2004), Century-scale movement of the Atlantic Intertropical Convergence Zone linked to solar variability, *Geophys. Res. Lett.*, *31*, L12214, doi:10.1029/2004GL019940.

Poveda, G., and O. J. Mesa (1997), Feedbacks between hydrological processes in tropical South America and large-scale ocean-atmospheric phenomena, *J. Clim.*, *10*(10), 2690–2702, doi:10.1175/1520-0442(1997)010<2690:FBHPIT>2.0.CO;2.

Reimer, P. J., et al. (2004), IntCal04 terrestrial radiocarbon age calibration, 0–26 cal kyr BP, *Radiocarbon*, *46*(3), 1029–1058.

Richey, J. N., R. Z. Poore, B. P. Flower, T. M. Quinn, and D. J. Hollander (2009), Regionally coherent Little Ice Age cooling in the Atlantic Warm Pool, *Geophys. Res. Lett.*, *36*, L21703, doi:10.1029/2009GL040445.

Roth, S., and J. G. Reijmer (2005), Holocene millennial to centennial carbonate cyclicity recorded in slope sediments of the Great Bahama Bank and its climatic implications, *Sedimentology*, *52*, 161–181, doi:10.1111/j.1365-3091.2004.00684.x.

Saenger, C., P. Chang, L. Ji, D. W. Oppo, and A. L. Cohen (2009), Tropical Atlantic climate response to low-latitude and extratropical sea-surface temperature: A Little Ice Age perspective, *Geophys. Res. Lett.*, *36*, L11703, doi:10.1029/2009GL038677.

Schmidt, G. A., G. R. Bigg, and E. J. Rohling (1999), Global Seawater Oxygen-18 Database, http://data.giss.nasa.gov/data/, Goddard Inst. for Space Stud., New York.

Schmidt, M. W., H. J. Spero, and D. W. Lea (2004), Links between salinity variation in the Caribbean and North Atlantic thermohaline circulation, *Nature*, *428*, 160–163, doi:10.1038/nature02346.

Schmidt, M. W., M. J. Vautravers, and H. J. Spero (2006), Rapid subtropical North Atlantic salinity oscillations across Dansgaard-Oeschger cycles, *Nature*, *443*, 561–564, doi:10.1038/nature05121.

Schmittner, A., and A. C. Clement (2002), Sensitivity of the thermohaline circulation to tropical and high latitude freshwater forcing during the last glacial- interglacial cycle, *Paleoceanography*, *17*(2), 1017, doi:10.1029/2000PA000591.

Schmittner, A., C. Appenzeller, and T. F. Stocker (2000), Enhanced Atlantic freshwater export during El Nino, *Geophys. Res. Lett.*, *27*(8), 1163–1166, doi:10.1029/1999GL011048.

Schmitz, W. J., and P. L. Richardson (1991), On the sources of the Florida Current, *Deep Sea Res., Part A*, *38*, S379–S409.

Siddall, M., E. J. Rohling, A. Almogi-Labin, C. Hemleben, D. Meischner, I. Schmelzer, and D. A. Smeed (2003), Sea-level fluctuations during the last glacial cycle, *Nature*, *423*, 853–858, doi:10.1038/nature01690.

Spero, H. J., K. M. Mielke, E. M. Kalve, D. W. Lea, and D. K. Pak (2003), Multispecies approach to reconstructing eastern equatorial Pacific thermocline hydrography during the past 360 kyr, *Paleoceanography*, *18*(1), 1022, doi:10.1029/2002PA000814.

Stidd, C. K. (1967), The use of eigenvectors for climate estimates, *J. Appl. Meteorol.*, *6*, 255–264, doi:10.1175/1520-0450(1967)006<0255:TUOEFC>2.0.CO;2.

Sturges, W., and R. Leben (2000), Frequency of ring separations from the loop current in the Gulf of Mexico: A revised estimate, *J. Phys. Oceanogr.*, *30*(7), 1814–1819, doi:10.1175/1520-0485(2000)030<1814:FORSFT>2.0.CO;2.

Vonmoos, M., J. Beer, and R. Muscheler (2006), Large variations in Holocene solar activity: Constraints from ^{10}Be in the Greenland Ice Core Project ice core, *J. Geophys. Res.*, *111*, A10105, doi:10.1029/2005JA011500.

Vukovich, F. M. (1988), Loop Current boundary variations, *J. Geophys. Res.*, *93*(C12), 15,585–15,591, doi:10.1029/JC093iC12p15585.

Wagner, G., J. Masarik, J. Beer, S. Baumgartner, D. Imboden, P. W. Kubik, H. A. Synal, and M. Suter (2000), Reconstruction of the geomagnetic field between 20 and 60 kyr BP from cosmogenic radionuclides in the GRIP ice core, *Nucl. Instrum. Methods Phys. Res., Sect. B*, *172*, 597–604, doi:10.1016/S0168-583X(00)00285-8.

Waliser, D. E., and C. Gautier (1993), A satellite-derived climatology of the ITCZ, *J. Clim.*, *6*(11), 2162–2174, doi:10.1175/1520-0442(1993)006<2162:ASDCOT>2.0.CO;2.

Wang, P. X., S. Clemens, L. Beaufort, P. Braconnot, G. Ganssen, Z. M. Jian, P. Kershaw, and M. Sarnthein (2005), Evolution and variability of the Asian monsoon system: State of the art and outstanding issues, *Quat. Sci. Rev.*, *24*(5–6), 595–629, doi:10.1016/j.quascirev.2004.10.002.

Weldeab, S., R. R. Schneider, and M. Kölling (2006), Deglacial sea surface temperature and salinity increase in the western tropical Atlantic in synchrony with high latitude climate instabilities, *Earth Planet. Sci. Lett.*, *241*(3–4), 699–706, doi:10.1016/j.epsl.2005.11.012.

Weldeab, S., D. W. Lea, R. R. Schneider, and N. Andersen (2007), 155,000 years of West African monsoon and ocean thermal evolution, *Science*, *316*(5829), 1303–1307, doi:10.1126/science.1140461.